

Thermal equation of state and thermodynamic properties of iron carbide Fe₃C to 31 GPa and 1473 K

Konstantin D. Litasov,^{1,2} Igor S. Sharygin,^{1,2} Peter I. Dorogokupets,³ Anton Shatskiy,^{1,2} Pavel N. Gavryushkin,^{1,2} Tatiana S. Sokolova,³ Eiji Ohtani,⁴ Jie Li,⁵ and Kenichi Funakoshi⁶

Received 7 April 2013; revised 23 September 2013; accepted 3 October 2013; published 24 October 2013.

[1] Recent experimental and theoretical studies suggested preferential stability of Fe₃C over Fe₇C₃ at the condition of the Earth's inner core. Previous studies showed that Fe₃C remains in an orthorhombic structure with the space group *Pnma* to 250 GPa, but it undergoes ferromagnetic (FM) to paramagnetic (PM) and PM to nonmagnetic (NM) phase transitions at 6–8 and 55–60 GPa, respectively. These transitions cause uncertainties in the calculation of the thermoelastic and thermodynamic parameters of Fe₃C at core conditions. In this work we determined *P-V-T* equation of state of Fe₃C using the multianvil technique and synchrotron radiation at pressures up to 31 GPa and temperatures up to 1473 K. A fit of our *P-V-T* data to a Mie-Grüneisen-Debye equation of state produce the following thermoelastic parameters for the PM-phase of Fe₃C: $V_0 = 154.6$ (1) Å³, $K_{T0} = 192$ (3) GPa, $K_T' = 4.5$ (1), $\gamma_0 = 2.09$ (4), $\theta_0 = 490$ (120) K, and $q = -0.1$ (3). Optimization of the *P-V-T* data for the PM phase along with existing reference data for thermal expansion and heat capacity using a Kunc-Einstein equation of state yielded the following parameters: $V_0 = 2.327$ cm³/mol (154.56 Å³), $K_{T0} = 190.8$ GPa, $K_T' = 4.68$, $\Theta_{E10} = 305$ K (which corresponds to $\theta_0 = 407$ K), $\gamma_0 = 2.10$, $e_0 = 9.2 \times 10^{-5}$ K⁻¹, $m = 4.3$, and $g = 0.66$ with fixed parameters $m_{E1} = 3n = 12$, $\gamma_\infty = 0$, $\beta = 0.3$, and $a_0 = 0$. This formulation allows for calculations of any thermodynamic functions of Fe₃C versus *T* and *V* or versus *T* and *P*. Assuming carbon as the sole light element in the inner core, extrapolation of our equation of state of the NM phase of Fe₃C suggests that 3.3 ± 0.9 wt % C at 5000 K and 2.3 ± 0.8 wt % C at 7000 K matches the density at the inner core boundary.

Citation: Litasov, K. D., I. S. Sharygin, P. I. Dorogokupets, A. Shatskiy, P. N. Gavryushkin, T. S. Sokolova, E. Ohtani, J. Li, and K. Funakoshi (2013), Thermal equation of state and thermodynamic properties of iron carbide Fe₃C to 31 GPa and 1473 K, *J. Geophys. Res. Solid Earth*, 118, 5274–5284, doi:10.1002/2013JB010270.

1. Introduction

[2] F. Birch was among the first to recognize that the density of the Earth's liquid core is about 10% lower than the calculated density of iron at relevant PT-conditions [e.g., Birch, 1964]. During the following decades, the density and sound velocity profiles of the Earth's core have been determined with increasing precision. Simultaneously, the phase diagrams of iron and iron alloys have been studied

experimentally and theoretically at core pressures and temperatures. However, more recent estimations for the core density deficit are still approximately the same as those proposed by Birch [1964]. The density deficits vary from 5 to 12% for the outer core [Stevenson, 1981; Anderson and Isaak, 2002] and from 3 to 5% for the inner core [Stixrude et al., 1997; Dubrovinsky et al., 2000; Komabayashi and Fei, 2010; Yamazaki et al., 2012]. In addition to the density deficit, the core has lower sound velocities with respect to pure iron, which also provides evidence for light element addition [Fiquet et al., 2001; Lin et al., 2005]. The possible candidates for the light elements are H, C, O, Si, and S [Poirier, 1994; Li and Fei, 2003]. The value of the density deficit, the core-mantle boundary temperature, and quantitative estimations for light elements in the core can be constrained from various approaches. The thermodynamic analysis of equations of state (EOS) for iron and its compounds is one of the most important methods used to solve these problems.

[3] The Fe-C is a key system for understanding the composition of the core [Wood, 1993; Wood et al., 2013] and has been extensively studied over the past few decades. Experiments have been conducted to establish the Fe-C phase diagram at 1 bar or at high pressures using large-volume apparatus or diamond anvil cells. The 1 bar and large-volume data showed

¹Department of Geology and Geophysics, Novosibirsk State University, Novosibirsk, Russia.

²V.S. Sobolev Institute of Geology and Mineralogy, SB RAS, Novosibirsk, Russia.

³Institute of the Earth's Crust, SB RAS, Irkutsk, Russia.

⁴Department of Earth and Planetary Materials Science, Graduate School of Science, Tohoku University, Sendai, Japan.

⁵Department of Earth and Environmental Sciences, University of Michigan, Ann Arbor, Michigan, USA.

⁶Japan Synchrotron Radiation Research Institute, Kyoto, Hyogo, Japan.

Corresponding author: K. D. Litasov, Department of Geology and Geophysics, Novosibirsk State University, Novosibirsk, 630090, Russia. (klitasov@igm.nsc.ru)

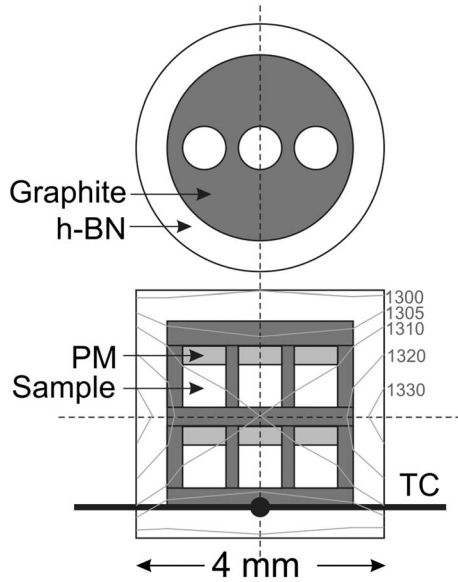


Figure 1. Six sample configurations in the cell assembly for TEL 12 mm. Only parts inside graphite heater with 4 mm inner diameter are shown. PM – pressure marker, TC – thermocouple. Grey lines show isotherms for experiment at 1300 K indicating less than 10 K differences across the samples (after *Shatskiy et al.* [2013]), which is confirmed by pressures measured by pressure markers.

that Fe_3C and Fe_7C_3 are the stable iron carbides up to 15 GPa [*Strong and Chrenko*, 1971; *Chipman*, 1972; *Chabot et al.*, 2008; *Nakajima et al.*, 2009]. Results from diamond anvil cell studies, however, have generated controversies concerning the stable form of iron carbide at the pressure and temperature conditions of the Earth’s core. *Lord et al.* [2009] suggested Fe_7C_3 as a principal carbide that is stable above 120 GPa based on extrapolation of their experiments on the Fe-C system performed at pressures up to 70 GPa. Taking the data from these experiments into account [*Nakajima et al.*, 2011] determined detailed P - V - T EOS of Fe_7C_3 at pressures up to 30 GPa and temperatures up to 1873 K and provided some constraints on the carbon content in the inner core. However, the most recent data available [*Takahashi et al.*, 2012] indicate the stability of Fe_3C at pressures up to 250 GPa and temperatures up to 4100 K, which specifies the possible importance of this carbide at pressure and temperature conditions found at the Earth’s core and also substantiated the analysis of the EOS too. The preferential stability of Fe_3C at 350 GPa is supported with theoretical calculation using the random structure search approach [*Weerasinghe et al.*, 2011]. Additional complications to the stable form of iron carbide at core conditions originate from ab initio simulation, which suggests the lowest formation enthalpy for Fe_2C phase at 300–400 GPa and 0 K [*Weerasinghe et al.*, 2011; *Bazhanova et al.*, 2012].

[4] The compressibility of iron carbides at 298 K has been determined up to 180 GPa [*Scott et al.*, 2001; *Li et al.*, 2002; *Sata et al.*, 2010; *Nakajima et al.*, 2011; *Chen et al.*, 2012]. The results of these experiments suggest that structures of Fe_3C (space group $Pnma$) and Fe_7C_3 (space group $P6_3mc$) remain the same up to 200–250 GPa. However, in addition to compositional variations, iron carbides undergo a range of second-order magnetic transitions. These magnetic transitions

may have approximately negligible effect on the unit cell volume, but affect the thermodynamic properties and elasticity of iron carbides. Fe_3C is a metallic ferromagnet (FM) at 1 bar and 298 K exhibiting the Invar effect with an extremely low coefficient of thermal expansion $\alpha = 1.3 \times 10^{-5} \text{ K}^{-1}$. The Curie temperature (T_C) is 480–485 K [*Tsuzuki et al.*, 1984; *Acet et al.*, 2001; *Wood et al.*, 2004], above which Fe_3C transforms into the paramagnetic phase (PM). The pressure of the transition from FM to PM and from PM to nonmagnetic phase (NM) is currently a topic of debate. In situ investigations probing atomic and electronic structure revealed the FM/PM transition occurred at 4.3–6.5 GPa by nuclear resonant scattering [*Gao et al.*, 2008], at 10 GPa by X-ray magnetic circular dichroism [*Duman et al.*, 2005], and at 25 GPa by X-ray emission spectroscopy (considered as FM/NM) [*Lin et al.*, 2004]. Other studies conducted on this topic have claimed a softening of phonon frequencies by inelastic X-ray scattering at 68 GPa [*Fiquet et al.*, 2009] and changes in lattice parameters at approximately 55 GPa by X-ray diffraction [*Ono and Mibe*, 2010]. Theoretical studies predicted that at 0 K, it loses its magnetic moment and undergoes a FM to NM transition at pressures above 60 GPa [*Vocadlo et al.*, 2002; *Mookherjee*, 2011] or 55 GPa [*Ono and Mibe*, 2010]. *Prescher et al.* [2012] performed single crystal measurements using Mossbauer spectroscopy and X-ray diffraction and placed the FM/PM transition at 8–10 GPa, the PM/NM transition at 22 GPa, and noticed the absence of electronic transitions until pressures of at least 55 GPa. The same transitions in Fe_7C_3 were detected at slightly different conditions. The T_C was observed at 523 K [*Tsuzuki et al.*, 1984], whereas the FM/PM transition at 298 K was observed at 18 GPa using X-ray diffraction and detected via change in a/c ratio of the hexagonal unit cell [*Nakajima et al.*, 2011]. Between 5.5 and 7.5 GPa, the FM/PM transition was determined using single crystal X-ray diffraction and Mossbauer spectroscopy [*Chen et al.*, 2012]. The PM/NM transition was observed at 53 GPa by analysis of the X-ray diffraction data and a/c ratio [*Chen et al.*, 2012]. Ab initio computations revealed the FM/NM transition at 67 GPa [*Mookherjee et al.*, 2011].

[5] Recognizing revived interest in Fe_3C as a potential carbide at Earth’s core conditions [*Weerasinghe et al.*, 2011; *Takahashi et al.*, 2012], here we present a P - V - T equation of state for Fe_3C up to 31 GPa and 1473 K with support from detailed thermodynamic analyses. The data can be used for thermodynamic modeling of chemical reactions with Fe_3C at upper-lower mantle conditions. Although the application to inner core conditions is complicated due to magnetic and electronic transitions in carbide, some constraints have been provided.

2. Experimental Methods

[6] The in situ X-ray diffraction experiments were conducted at the “Spring-8” synchrotron radiation facility (Japan), using Kawai-type multianvil apparatus, “SPEED-1500” [*Utsumi et al.*, 1998] and “SPEED-MkII” [*Katsura et al.*, 2004], installed at a bending magnet beam line BL04B1. An energy-dispersive X-ray diffraction technique was used for the in situ measurements. The incident X-rays were collimated to form a thin beam with dimensions of 0.05 mm in the horizontal direction and 0.1 mm in the vertical direction by WC slits and were positioned to the sample through a boron-epoxy window in a pyrophyllite gasket. The X-rays diffracted by the sample are

Table 1. Experimental Conditions and Unit Cell Parameters of Fe_3C Obtained by In Situ X-ray Diffraction^a

T (K)	V_{MgO} (\AA^3)	P_{MgO} (GPa)	a (\AA)	b (\AA)	c (\AA)	V (\AA^3)
<i>Run #1</i>						
1273	76.55(2)	2.26(4)	5.1360	6.8390	4.5600	160.17(1)
1073	75.78(2)	2.48(4)	5.1160	6.8040	4.5460	158.24(1)
873	75.10(2)	2.60(4)	5.0970	6.7770	4.5290	156.44(1)
673	74.42(2)	2.80(4)	5.0770	6.7550	4.5120	154.74(1)
573	74.23(2)	2.60(4)	5.0698	6.7488	4.5060	154.17(1)
523	74.11(2)	2.57(4)	5.0673	6.7453	4.5056	154.00(1)
473	74.01(2)	2.50(4)	5.0641	6.7399	4.5035	153.71(2)
423	73.93(2)	2.39(3)	5.0644	6.7366	4.5022	153.60(2)
373	73.84(2)	2.32(3)	5.0678	6.7313	4.5021	153.58(1)
300	73.68(2)	2.30(4)	5.0681	6.7272	4.5003	153.43(1)
673	74.82(3)	1.94(8)	5.0852	6.7630	4.5220	155.52(1)
573	74.53(3)	1.95(8)	5.0781	6.7525	4.5152	154.83(1)
523	74.46(3)	1.80(9)	5.0751	6.7476	4.5126	154.53(1)
473	74.32(3)	1.81(7)	5.0717	6.7439	4.5105	154.27(1)
423	74.20(3)	1.79(8)	5.0717	6.7407	4.5088	154.14(1)
373	74.12(3)	1.69(8)	5.0719	6.7387	4.5085	154.09(1)
300	73.95(1)	1.68(2)	5.0720	6.7350	4.5081	154.00(1)
300	74.56(2)	0.33(3)	5.0837	6.7477	4.5162	154.92(1)
373	74.74(2)	0.33(4)	5.0845	6.7503	4.5184	155.08(1)
423	74.85(3)	0.38(6)	5.0852	6.7522	4.5205	155.22(1)
473	75.00(2)	0.35(4)	5.0849	6.7569	4.5203	155.31(1)
523	75.07(3)	0.50(6)	5.0891	6.7597	4.5231	155.60(1)
573	75.24(2)	0.45(3)	5.0926	6.7655	4.5263	155.95(1)
673	75.46(3)	0.62(7)	5.0990	6.7740	4.5320	156.54(1)
873	76.10(3)	0.60(8)	5.1130	6.7990	4.5430	157.93(1)
1073	76.64(2)	0.84(6)	5.1270	6.8230	4.5590	159.48(1)
1273	77.37(2)	0.78(4)	5.1510	6.8570	4.5770	161.66(1)
473	75.06(2)	0.23(4)	5.0873	6.7588	4.5223	155.49(1)
300		0	5.0878	6.7512	4.5197	155.25(1)
<i>Run #2</i>						
300	71.69(1)	7.23(2)	5.029	6.664	4.463	149.57(1)
1473	75.23(2)	6.07(4)	5.117	6.817	4.538	158.30(1)
1373	74.83(2)	6.30(5)	5.109	6.802	4.528	157.35(1)
1273	74.50(2)	6.37(4)	5.101	6.778	4.516	156.14(2)
1173	74.18(2)	6.45(4)	5.096	6.750	4.514	155.27(2)
1073	73.88(1)	6.48(3)	5.086	6.736	4.508	154.44(1)
873	73.33(1)	6.50(2)	5.070	6.719	4.499	153.26(1)
673	72.78(1)	6.58(2)	5.057	6.705	4.488	152.18(2)
473	72.25(1)	6.71(2)	5.042	6.687	4.475	150.88(1)
<i>Run #3</i>						
300		0	5.085	6.751	4.521	155.20(2)
1473	73.26(2)	10.4(1)	5.088	6.761	4.499	154.77(2)
1273	72.71(2)	10.5(1)	5.069	6.731	4.484	152.99(2)
1073	72.06(3)	10.9(1)	5.054	6.702	4.475	151.58(2)
873	71.71(1)	10.5(1)	5.039	6.681	4.470	150.49(2)
673	71.45(3)	10.0(1)	5.030	6.672	4.461	149.71(2)
473	71.17(2)	9.6(1)	5.021	6.657	4.451	148.77(2)
300	70.92(3)	9.3(1)	5.012	6.641	4.446	147.98(2)
<i>Run #4</i>						
300		0	5.084	6.744	4.524	155.11(2)
300	67.94(4)	18.6(1)	4.952	6.559	4.389	142.56(2)
1473	70.64(2)	17.2(1)	5.038	6.680	4.449	149.73(2)
1273	69.98(2)	17.9(1)	5.025	6.643	4.432	147.94(2)
1073	69.81(2)	17.1(1)	5.018	6.631	4.427	147.31(2)
1073	69.38(2)	18.4(1)	5.012	6.619	4.422	146.70(2)
873	69.66(2)	16.3(1)	5.011	6.623	4.424	146.82(2)
873	68.84(2)	18.9(1)	4.987	6.592	4.413	145.07(2)
673	69.54(3)	15.5(1)	4.997	6.618	4.427	146.40(2)
473	69.43(3)	14.7(1)	4.985	6.611	4.422	145.73(2)
300	69.36(3)	14.0(1)	4.980	6.601	4.417	145.20(2)
<i>Run #5</i>						
1473	68.26(3)	24.5(1)	4.994	6.622	4.408	145.77(2)
1273	67.90(2)	24.5(1)	4.981	6.601	4.397	144.57(2)
1073	67.70(4)	24.0(1)	4.971	6.588	4.391	143.80(2)
873	67.47(4)	23.6(1)	4.962	6.571	4.385	142.97(2)
673	67.28(3)	23.0(1)	4.955	6.558	4.382	142.39(2)
473	67.08(3)	22.6(1)	4.944	6.543	4.373	141.46(2)
300	67.05(3)	21.8(1)	4.936	6.536	4.368	140.92(2)
300	67.15(2)	21.4(1)	4.937	6.536	4.372	141.08(2)

Table 1. (continued)

T (K)	V_{MgO} (Å ³)	P_{MgO} (GPa)	a (Å)	b (Å)	c (Å)	V (Å ³)
Run #6						
673	65.23(5)	31.0(2)	4.908	6.503	4.340	138.52(2)
873	65.66(5)	30.5(2)	4.919	6.515	4.353	139.50(2)
1073	65.92(2)	30.6(1)	4.928	6.521	4.365	140.27(2)
1273	66.22(2)	30.7(1)	4.943	6.544	4.369	141.32(2)
1473	66.46(2)	31.0(1)	4.954	6.561	4.377	142.27(2)
1273	66.67(2)	29.0(1)	4.953	6.557	4.375	142.09(2)
1073	66.08(2)	30.0(1)	4.932	6.529	4.366	140.59(2)
873	65.85(4)	29.7(1)	4.923	6.520	4.353	139.72(2)
673	65.61(3)	29.4(1)	4.916	6.512	4.348	139.19(2)
473	65.47(5)	28.9(2)	4.906	6.499	4.341	138.41(2)
300	65.31(4)	28.6(1)	4.898	6.486	4.332	137.62(2)
Run #7						
1473	71.05(2)	16.1(1)	5.048	6.701	4.459	150.83(2)
1373	70.79(2)	16.1(1)	5.044	6.681	4.449	149.93(2)
1273	70.75(2)	15.6(1)	5.041	6.667	4.446	149.42(2)
1273	70.53(4)	16.3(1)	5.035	6.661	4.440	148.91(2)
1073	70.44(3)	15.3(1)	5.033	6.654	4.437	148.59(2)

^aRun #7 includes measurements from several runs on carbonate-iron interaction experiments (unpublished data). The 1 σ errors are in parentheses, they are not shown for unit cell dimensions (<0.001 Å). Pressure was calculated using MgO EOS in Sokolova *et al.* [2013].

detected by a pure Ge solid state detector with a 4096 multichannel analyzer. The analyzer was calibrated by using characteristic X-rays of Cu, Mo, Ag, La, Ta, Pt, Au, and Pb. The diffraction angle (2θ) was approximately 5.5° , was calibrated before compression using the known d values of X-ray diffraction peaks of MgO (note volumes used in the beam line software, $V_0 = 71.778 \text{ \AA}^3$), with an uncertainty of less than 0.0005° . In “SPEED-MkII,” an oscillation system was used to obtain more accurate X-ray powder diffraction patterns at high temperature by oscillating the press from -3° to 6° in horizontal plane. A detailed description of the press system and performance of the oscillation is given by [Katsura *et al.*, 2004].

[7] Fine-grained Fe₃C powder (99.9%, Rare Metallic Co. Ltd.) was prepared as the starting material. We used 26 mm WC anvils with different truncation edge lengths (TEL) for the experiments. In runs #1 and #2 (TEL 12 mm) we investigated six starting materials (Figure 1), including Fe₃C, placed separately in a graphite capsule and adjusted with a MgO pressure marker (Table 1). In runs #3 and #4 (TEL 5.0 and 3.5 mm, respectively), we investigated Fe₃C and Fe₃N together in the same graphite capsule (Figure 2). These materials were separated by a MgO plate which served as a pressure marker. The X-ray probed area within the pressure marker and the sample are about 20 μm apart, and their temperatures differ by no more than 10 K. In runs #5 and #6 (TEL 2.0 mm), a pressure marker composed of a fine mixture of Au and MgO (1:15) was placed symmetrically to the Fe₃C sample in relation to the temperature field of the cell (Figure 2). The sample and the Au-MgO pressure marker were separated by a thin graphite plate. Also, some data on the volume of Fe₃C were obtained from several unpublished carbonate-iron reaction experiments at 15–17 GPa and were used to supplement the data collected in run #7 (Table 1). The sample configuration in run #7 was the same as in runs #5 and #6.

[8] The sample assembly at 20–31 GPa was similar to that reported by Litasov *et al.* [2005, 2008], and consisted of a Co-doped MgO pressure medium, a cylindrical LaCrO₃ heater, molybdenum electrodes, and a graphite sample capsule. Lower pressure (<20 GPa) cell assembly included a ZrO₂

pressure medium with a diamond powder insert with MgO caps (for X-ray transparency) and a LaCrO₃ or graphite heater. The graphite heater was separated from the graphite sample capsule by a thin BN sleeve. Temperature was monitored by a W_{97%}Re_{3%}-W_{75%}Re_{25%} thermocouple with a junction located at nearly the same position as where the X-rays pass through the sample. This minimized the effect of the thermal gradient across the sample chamber on temperature measurements. The effect of pressure on thermocouple electromotive forces (emf) was ignored during experiments.

[9] The P - T conditions of the experiments are summarized in Figure 3. In all runs we performed compression with either one or two subsequent heating cycles. The exposure times for collecting diffraction data were between 200 and 400 s. The experimental pressures at high temperature were calculated from the unit cell volume of MgO using the optimized EOS presented in Litasov *et al.* [2013] and Sokolova *et al.* [2013].

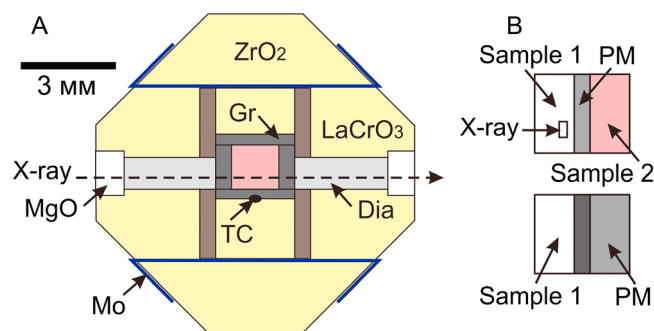


Figure 2. (a) Cell assembly for TEL 5.0 mm and (b) schematic sample configurations in the assemblies for TEL 5.0, 3.5, and 2.0 mm. In Figure 2b, top scheme shows configuration for two samples separated by PM (e.g., Fe₃C, Fe₃N, and MgO-pressure marker). Figure 2b, bottom scheme shows configuration for one sample and pressure marker separated by a plate from capsule material (e.g., Fe₃C and MgO + Au pressure marker in graphite capsule). X-ray path or window is indicated in the drawing, Gr – graphite, Dia – diamond powder, TC – thermocouple.

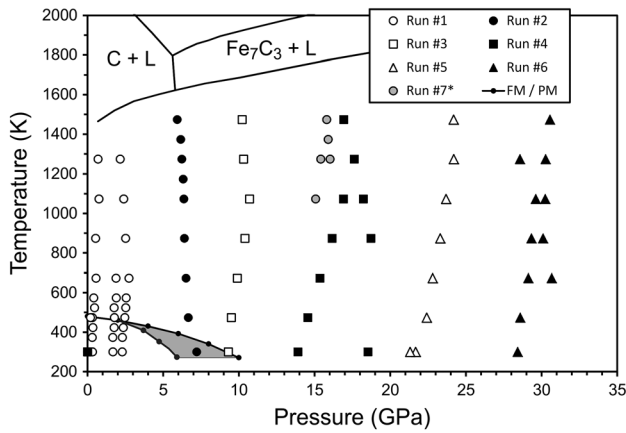


Figure 3. Pressure-temperature conditions of in situ X-ray diffraction experiments for Fe_3C . The pressures were calculated using MgO EOS. Phase diagram is after Nakajima *et al.* [2009]. *Run #7 includes several measurements from Fe-carbonate interaction experiments resulting in formation of Fe_3C (unpublished data). The boundary between FM and PM phase is based on data by Wood *et al.* [2004] at 1 bar, this work, and at 300 K with uncertainty shown as a grey field according to Gao *et al.* [2008] and Prescher *et al.* [2012].

This pressure scale was similar to that reported in Dorogokupets and Dewaele [2007] and Dorogokupets and Oganov [2007] with <0.3 GPa differences at 30 GPa and high temperatures. Typically, 4–5 diffraction lines (111), (200), (220), (311), and (222) of MgO were used to calculate pressure, and up to 20 major diffraction lines were used to calculate the volume of Fe_3C (Figure 4). We refined the X-ray diffraction patterns to determine the d values using the “XRayAnalysis” software provided by the beam line. The uncertainties of the unit cell volume of MgO were determined by a least-squares fit method and yielded typical values of less than 0.1 GPa uncertainty in pressure.

[10] The quality of the diffraction patterns and the deviation from the hydrostatic conditions during the experiment were determined using FWHM (full width at half maximum) of X-ray diffraction lines. The FWHM of X diffraction lines of Fe_3C and MgO at the maximum pressure and high temperature were below 10 keV, identical to those at 0.0001–3.0 GPa after heating. This indicated that differential stress was nearly relaxed by high-temperature annealing at all pressures. The precision of the experiments was confirmed by consistent results obtained using various cell configurations in different runs.

3. Equation of State

[11] We used two conventional approaches to calculate thermoelastic parameters for Fe_3C : (a) a high-temperature (HT) EOS and (b) a Mie-Grüneisen-Debye (MGD) EOS. The formalism for these approaches can be found in the literature [Anderson, 1995; Jackson and Rigden, 1996; Poirier, 2000; Litasov *et al.*, 2007]. For 298 K isotherm, we used the Vinet-Rydberg (VR) EOS [Vinet *et al.*, 1987]. In addition, we performed a thermodynamic analysis of EOS based on the formalism proposed by Dorogokupets *et al.* [Dorogokupets and Dewaele, 2007; Dorogokupets and Oganov, 2007; Litasov *et al.*, 2013; Sokolova *et al.*, 2013]. We named this

approach as a Kunc-Einstein (KE) EOS. The detailed formalism is presented by Litasov *et al.* [2013], and we note here only some modifications and details.

[12] The Kunc EOS for room-temperature isotherm with parameter $k=2$ is equal to Vinet/Rydberg EOS [Kunc *et al.*, 2003], so we used a similar equation in all three approaches. The full solution allowed us to find all the necessary parameters for KE EOS, which include: V_0 – volume at standard conditions, K_{T0} – isothermal bulk modulus and K_T' – its pressure derivative, Θ_{E10} and Θ_{E20} – two characteristic temperatures, $m_{E1}=m_{E2}=3n$ – number of atoms in a formula unit, γ_0 and γ_∞ – Grüneisen parameters at ambient conditions and infinite compression, β – power-mode parameter in Grüneisen equation, e_0 – parameter, which denotes an electronic contribution to the free energy, a_0 – intrinsic anharmonicity parameter, m – which is an anharmonicity equivalent of the Grüneisen parameter, and g – which is an electronic equivalent of the Grüneisen parameter. In this work we simplified this approach to use one characteristic temperature taking into account scarce data for thermochemistry and elasticity of PM Fe_3C at ambient conditions. With the described formalism, we can calculate any thermodynamic functions versus T and V or versus T and P . The procedure for optimization of the thermodynamic parameters for EOS was also described previously [Dorogokupets and Oganov, 2007].

4. Results

[13] The measured unit cell parameters of FM Fe_3C before and after experiments ($a=5.086$ Å, $b=6.749$ Å, $c=4.522$ Å, and $V=155.2$ (1) Å³) are consistent with previous data [Li *et al.*, 2002; Wood *et al.*, 2004]. The analysis of X-ray diffraction data began with determination of the magnetic transitions, which can significantly affect the calculated thermoelastic parameters if all of the data were considered together. The FM/PM transition can be successfully monitored using the calculated unit cell volume, and specifically the parameter a (Figure 5). The temperature dependence of the a value changes from the FM to the PM phase and marks the T_C value. We observed a minor decrease of T_C in the pressure interval from 0.3 to 3 GPa and found consistent results with neutron diffraction data at 1 bar [Wood *et al.*, 2004].

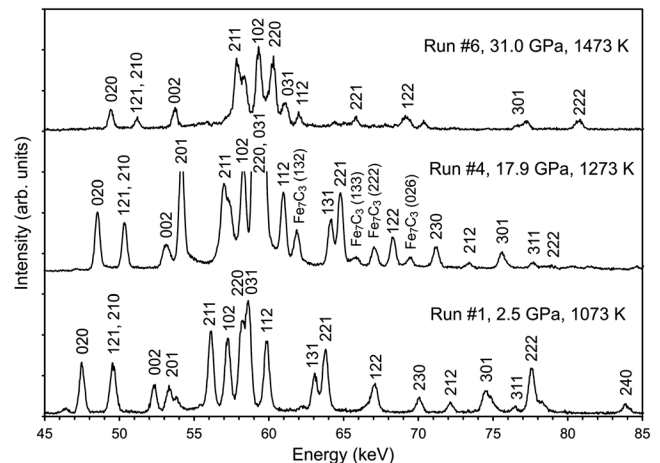


Figure 4. Representative X-ray diffraction patterns of Fe_3C at different pressures.

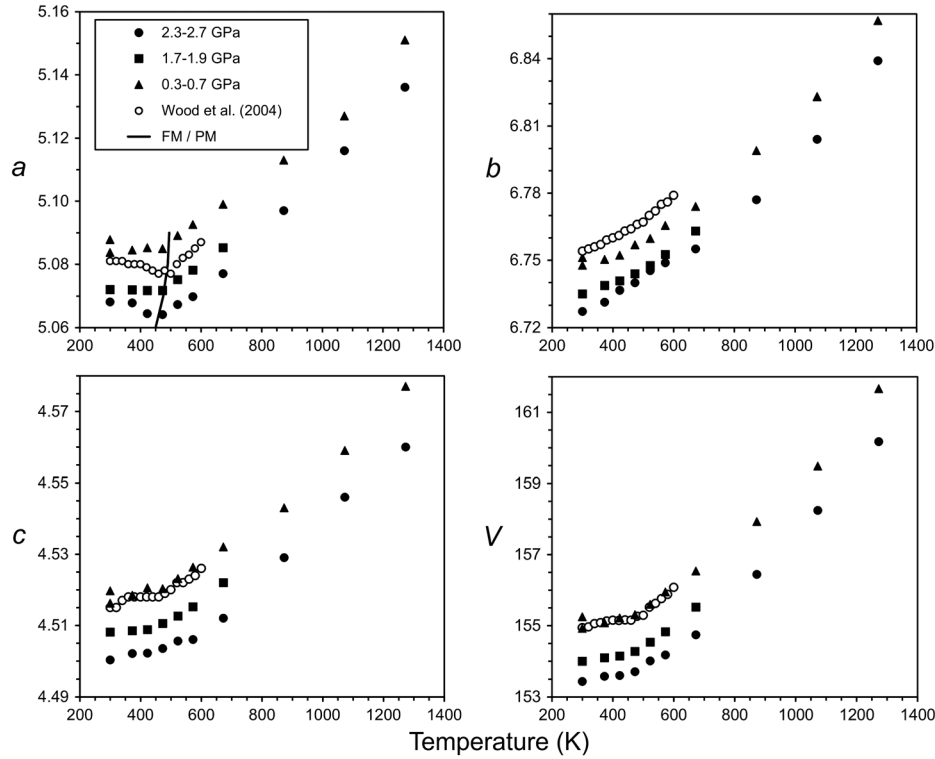


Figure 5. Temperature dependence of volume and unit cell parameters of Fe₃C at pressures below 3 GPa.

The pressure of the FM/PM transition may be located between 7.2 and 9.3 GPa; however, the data point at 7.2 GPa cannot be considered as significantly deviated from the 298 K compression curve (Figure 6), which is consistent with the data by *Gao et al.* [2008] and *Prescher et al.* [2012]. The transition from the PM to NM phase suggested by *Prescher et al.* [2012] at 22 GPa and 298 K cannot be precisely determined from our data. The data at 28–31 GPa are generally consistent with the fit of other data for the PM phase (Figure 6), whereas the volume of Fe₃C at 28.6 GPa may correspond to the compression curve of both the PM phase

(this work) and the NM phase, if we plot the data from *Sata et al.* [2010] (Figure 6). The position of the PM/NM transition at high temperatures is unknown, because it can be structurally hidden. From our data we can conclude that the thermal properties of the PM and the NM phases may be close to each other if the NM phase is stable at 20–31 GPa and high temperatures. We observed only minor deviations of the volumes from the

Table 2. Comparison of the Volume and Bulk Modulus Data for Fe₃C

Phase	V_{0T} (Å ³)	K_{T0} (GPa)	K'_T	P Range (GPa)	EOS	Ref
<i>Experiments, 298 K</i>						
FM	155.2	175	5 ^b	0–7.2	VR	This work
PM	154.56	190 (2)	4.8 (1)	0–31	VR	This work, HT ^c
PM	154.42	194(1)	4.6(1)	0–31	VR	This work, MGD ^c
PM	154.56	191 (2)	4.68 (8)	0–31	VR	This work, KE ^c
---	155.3	168 (3)	5.8 (3)	0–31	VR	<i>Li et al.</i> [2002]
FM	155.4	166 (6)	6.7 (3)	14–35	VR	<i>Ono and Mibe</i> [2010]
PM	154.2	145 (3)	8.5 (7)	8–22	BM	<i>Prescher et al.</i> [2012]
NM	148.5	316 (6)	3.5 (1)	50–184	VR	<i>Sata et al.</i> [2010]
<i>Calculations, 0 K</i>						
FM	153.3	173	5.8		BM	<i>Vocadlo et al.</i> [2002]
FM	152.0	212	4.5			<i>Huang et al.</i> [2005]
FM	151.9	216	4.15	0–35	BM	<i>Ono and Mibe</i> [2010]
FM	151.6	183	6.0		VR	<i>Mookherjee</i> [2011]
NM	148.9	317	4.3		BM	<i>Vocadlo et al.</i> [2002]
NM	149.5	322	3.7			<i>Huang et al.</i> [2005]
NM	142.5	316	4.4	<400	BM	<i>Ono and Mibe</i> [2010]
NM	143.2	297	4.9		VR	<i>Mookherjee</i> [2011]

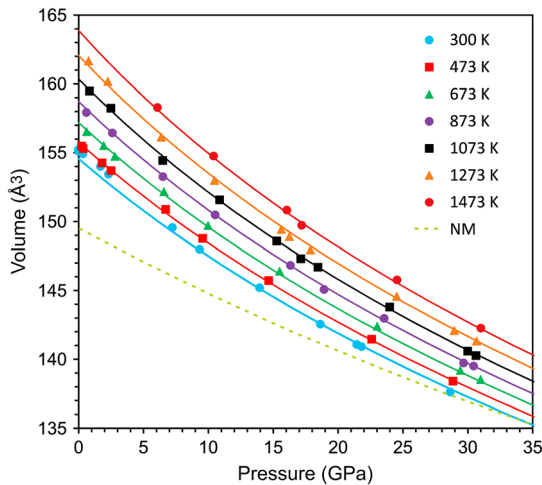


Figure 6. KE EOS fit to P - V - T data for Fe₃C. Solid lines are isothermal compression curves at 300, 473, 673, 873, 973, 1073, 1273, and 1473 K. The dashed line shows the compression curve of the NM phase of Fe₃C [*Sata et al.*, 2010].

^aNot specified.

^bFixed value.

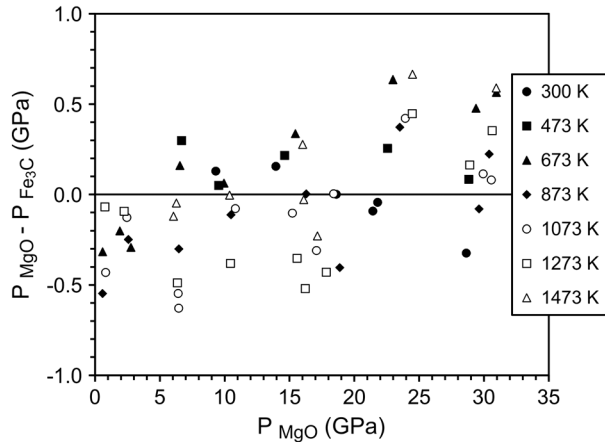
^cSee text for thermal parameters. The EOSes for pressure markers used in original works were recalculated to Ruby or MgO scale from *Sokolova et al.* [2013]. BM – Birch-Murnaghan EOS, VR – Vinet-Rydborg EOS.

Table 3. Calculated Thermodynamic Parameters for PM Phase of Fe_3C at Different Pressures and Temperatures Using KE EOS

P (GPa)	T (K)	$x=V/V_0$	$\alpha \times 10^{-5}$ (K^{-1})	S	C_P ($\text{J mol}^{-1} \text{K}^{-1}$)	C_V	K_T (GPa)	K_S (GPa)	γ	ΔG (KJ mol^{-1})
0.0001	298.15	1.0000	4.36	104.48	96.76	94.25	190.8	195.9	2.096	0.002
0.0001	500	1.0093	4.80	157.13	106.42	101.47	183.5	192.4	2.102	-26.775
0.0001	1000	1.0355	5.44	235.32	120.26	108.50	165.0	182.8	2.118	-126.736
0.0001	1500	1.0659	6.14	286.67	134.32	113.87	145.9	172.1	2.137	-257.861
0.0001	2000	1.1015	7.05	327.55	151.36	119.21	126.1	160.1	2.158	-411.702
10	298.15	0.9541	3.58	95.53	94.49	92.49	236.0	241.1	2.067	227.129
10	500	0.9614	3.95	147.19	104.67	100.68	228.9	238.0	2.072	202.272
10	1000	0.9818	4.40	223.90	117.34	108.01	211.4	229.7	2.085	107.662
10	1500	1.0046	4.82	273.65	128.99	113.25	193.5	220.4	2.099	-17.367
10	2000	1.0303	5.31	312.50	142.02	118.33	175.2	210.2	2.115	-164.212
20	298.15	0.9177	3.06	88.34	92.48	90.82	278.6	283.6	2.043	444.765
20	500	0.9237	3.40	139.17	103.31	99.94	271.7	280.9	2.047	421.456
20	1000	0.9405	3.75	214.84	115.44	107.60	254.8	273.4	2.058	331.128
20	1500	0.9590	4.05	263.59	125.78	112.76	237.6	265.0	2.070	210.873
20	2000	0.9793	4.37	301.27	136.86	117.67	220.1	256.0	2.083	69.339
30	298.15	0.8874	2.68	82.33	90.63	89.21	319.3	324.4	2.023	654.690
30	500	0.8926	3.01	132.42	102.17	99.23	312.6	321.9	2.026	632.681
30	1000	0.9069	3.30	207.29	114.05	107.23	296.1	314.9	2.036	545.944
30	1500	0.9225	3.53	255.33	123.57	112.35	279.3	307.2	2.046	429.640
30	2000	0.9395	3.77	292.22	133.47	117.14	262.4	298.9	2.057	292.429
40	298.15	0.8616	2.40	77.17	88.90	87.66	358.7	363.7	2.005	858.122
40	500	0.8661	2.71	126.59	101.15	98.55	352.1	361.4	2.008	837.234
40	1000	0.8786	2.97	200.78	112.96	106.89	335.8	354.9	2.016	753.598
40	1500	0.8922	3.16	248.29	121.92	112.00	319.4	347.7	2.026	640.680
40	2000	0.9068	3.35	284.60	131.01	116.69	302.8	340.0	2.036	507.133

isothermal fitting curves at 21–24.5 and 28.6–31 GPa. Because the values of the isothermal fitting curves were closely related in this work, we analyzed them together.

[14] It was difficult to determine a compressibility curve for PM-phase from our data at 298 K, because it included only five data points in a narrow pressure interval of 9–22 GPa with uncertain V_0 . Therefore, we combined the analysis of the 298 K isotherm with the high-temperature data. The results of the fitting of the P - V - T data using different approaches are presented in Tables 2 and 3 and plotted in Figure 6. Calculated residual pressures showed no systematic errors in the measurements with a maximum deviation of 0.7–0.8 GPa (Figure 7), which indicates relatively high precision and consistency within the results. A least-square fit to HT-VR EOS yields $V_0 = 154.5 \pm 0.1 \text{ \AA}^3$, $K_{T0} = 190 \pm 3 \text{ GPa}$,

**Figure 7.** Differences between pressures calculated using EOS of MgO pressure standards and pressures calculated using KE EOS for PM Fe_3C .

and $K_T' = 4.8 \pm 0.2$. Thermal parameters include $(\partial K_T / \partial T)_P = -0.029 \pm 0.002 \text{ GPa/K}$ and thermal expansion $\alpha = a_0 + a_1 T$ with $a_0 = 3.90 (\pm 0.15) \times 10^{-5} \text{ K}^{-1}$ and $a_1 = 1.22 (\pm 0.17) \times 10^{-8} \text{ K}^{-2}$. In comparison, extrapolation of 1 bar measurements of *Wood et al.* [2004] at 460–600 K to the lower temperatures yields $V_0 = 154.14 \text{ \AA}^3$ and calculated $\alpha = 4.1 \times 10^{-5} \text{ K}^{-1}$. The analysis of the compression curve for the PM phase in previous works was considered only along with the FM phase (Figure 8) and revealed parameters shown in Table 2. Fitting of our data to MGD relation yielded $\gamma_0 = 2.15 \pm 0.03$ and $q = -0.03 \pm 0.27$ and the Debye temperature, $\theta_0 = 314 \pm 120 \text{ K}$. Usually, θ_0 is poorly resolvable from the high-pressure P - V - T data; however, there are no reported reference values for the

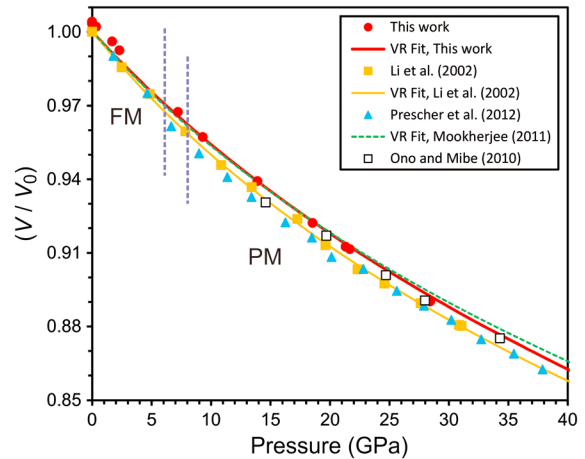
**Figure 8.** The compression curve of Fe_3C along the 298 K isotherm (solid circle) fitted to a VR EoS (solid curve). The dashed lines denote boundaries between the FM and PM phases according to *Gao et al.* [2008] and *Prescher et al.* [2012].

Table 4. Relative Volumes (V/V_0) of PM Fe₃C as a Function of Pressure and Temperature Using KE EOS^a

P (GPa)	T (K)							
	298.15	500	750	1000	1250	1500	1750	2000
0.0001	1.0000	1.0093	1.0220	1.0355	1.0501	1.0659	1.0829	1.1015
5	0.9756	0.9838	0.9948	1.0066	1.0192	1.0326	1.0470	1.0624
10	0.9541	0.9614	0.9713	0.9818	0.9929	1.0046	1.0171	1.0303
15	0.9350	0.9416	0.9505	0.9599	0.9699	0.9804	0.9914	1.0031
20	0.9177	0.9237	0.9319	0.9405	0.9495	0.9590	0.9689	0.9793
25	0.9019	0.9075	0.9150	0.9229	0.9312	0.9398	0.9489	0.9583
30	0.8874	0.8926	0.8996	0.9069	0.9145	0.9225	0.9308	0.9395
35	0.8741	0.8789	0.8854	0.8922	0.8993	0.9067	0.9144	0.9224
40	0.8616	0.8661	0.8722	0.8786	0.8853	0.8922	0.8993	0.9068

$$^a V_0 = 154.56 \text{ \AA}^3.$$

PM phase of Fe₃C. Reported θ_0 for (presumably) FM phase determined by different methods was 394 K [Gustafson, 1985], 420–450 K [Belikov and Savinskaya, 1962], 468–475 K [Dodd *et al.*, 2003], and 604 K [Wood *et al.*, 2004]. If we fix θ_0 at 500 K, the γ_0 calculated from our data will be 2.13 ± 0.02 and $q = -0.36 \pm 0.23$. The thermal Grüneisen parameter calculated by Wood *et al.* [2004] was $\gamma_0 = 2.1$. Optimization of the P - V - T data for the PM phase along with the reference data for thermal expansion and heat capacity using KE EOS yields the following parameters: $V_0 = 2.327 \text{ cm}^3/\text{mol}$ (154.56 \AA^3), $K_{T0} = 190.8 \text{ GPa}$, $K_T' = 4.68$, $\Theta_{E10} = 305$ (which correspond to $\theta_0 = 407 \text{ K}$), $\gamma_0 = 2.10$, $e_0 = 9.2 \times 10^{-5} \text{ K}^{-1}$, $m = 4.3$, and $g = 0.66$. Fixed parameters include: $m_{E1} = 3n = 12$, $\gamma_\infty = 0$, $\beta = 0.3$, and $a_0 = 0$. Calculated thermoelastic and thermochemical parameters using KE EOS for PM Fe₃C are listed in Tables 3 and 4.

[15] Axial compressibility of PM Fe₃C at 298 K is shown in Figure 9. The VR EOS fit with fixed $K_T' = 4.8$ revealed limited axial anisotropy of compressibility for PM Fe₃C. We obtained $a_0 = 5.085 \text{ \AA}$, $b_0 = 6.743 \text{ \AA}$, $c_0 = 4.523 \text{ \AA}$, and $K_{T0a} = 195$ (2) GPa, $K_{T0b} = 186$ (3) GPa, $K_{T0c} = 163$ (2) GPa.

[16] Finally, we note that fitting of limited volume data at pressures below 8 GPa for the FM phase using VR EOS yields $V_0 = 155.27 \pm 0.05 \text{ \AA}^3$, and $K_T = 175 \pm 2 \text{ GPa}$, if K_T' is fixed at 5.

5. Discussion

5.1. Thermoelastic and Thermochemical Properties of Fe-Carbide

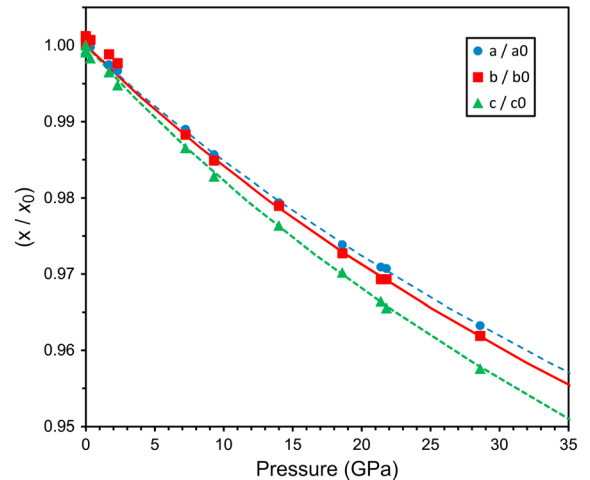
[17] In order to constrain the thermodynamic properties of PM Fe₃C, we applied the KE EOS and formalism described in Litasov *et al.* [2013] and Sokolova *et al.* [2013]. Thermodynamic data for Fe₃C at 1 bar are complicated due to the magnetic transition. Thermochemical data for PM Fe₃C are summarized in Barin [1995] and Hallstedt *et al.* [2010]. The thermal expansion data are available for the temperature range of 480–700 K [Jellinghaus, 1966; Kagawa and Okamoto, 1983; Wood *et al.*, 2004]. The coefficient of thermal expansion and the temperature dependence of the unit cell volume determined by Kagawa and Okamoto [1983] and Wood *et al.* [2004] are generally consistent with the calculated values from our data (Figures 10a and 10b). The calculated heat capacity is also fairly consistent with experimental and theoretical data for C_P (Figure 10c). Similar minor deviation can be noted for the calculated entropy and the Gibbs free energy, $S_{0,500} = 157.1 \text{ J}/(\text{mol K})$ and $\Delta G_{0,500} = -26.8 \text{ kJ}/\text{mol}$ in this work and $S_{0,500} = 177.6 \text{ J}/$

(mol K) and $\Delta G_{0,500} = -33.7 \text{ kJ}/\text{mol}$ in Barin [1995]. The temperature dependence of the bulk moduli is shown in Figure 10d. Calculated pressure dependence of the bulk moduli can be compared with data obtained by inelastic X-ray scattering (IXRS) (Figure 11). The data for K_T/K_S calculated for FM and PM phases are consistent with those obtained by IXRS [Gao *et al.*, 2008; 2011]. Although at pressures above 25 GPa the data on K_S calculated from IXRS [Gao *et al.*, 2011] deviate slightly (following linear trend) toward a higher bulk modulus, they remain significantly lower than estimations of K_T from X-ray diffraction measurements by Sata *et al.* [2010] for NM-Fe₃C.

[18] The unit cell volumes of the PM and NM phases are very similar at 25–30 GPa, and the differences in volumes at 200 GPa are about 1.5–1.7% (Figure 12). In this diagram we should note significant differences in volume and compressibility between single crystal [Prescher *et al.*, 2012] and powder diffraction data [Ono and Mibe, 2010] for Fe₃C. Nevertheless, certain uncertainties remain about PM/NM phase transition at high pressures. Although Prescher *et al.* [2012] argued for the PM/NM transition at 22 GPa, in the work by Ono and Mibe [2010] and in theoretical calculations [Mookherjee, 2011], this magnetic transition (named as FM/NM) was observed at 55–60 GPa. If the PM/NM transition occurs at 22 GPa [Prescher *et al.*, 2012], what would be the reason for the observed significant unit cell volume drop [Ono and Mibe, 2010] at 55 GPa? The authors of newer work [Prescher *et al.*, 2012] did not comment on this matter. Thus, this uncertainty should be clarified in future studies. In this work we followed the higher-pressure PM/NM transition data by Ono and Mibe [2010], who showed a prominent volume change at 55 GPa (Figure 12).

5.2. Implication for the Inner Core

[19] Data for EOS of Fe-carbides can be compared with density and sound velocity data for the inner core. For this purpose we need large extrapolation of the data obtained at lower pressures. For both Fe-carbides, Fe₇C₃ and Fe₃C, the EOS for the PM phase is obtained for a pressure range of 0–30 GPa. However, thermodynamic data for the PM phase of Fe₃C cannot be directly applied to model NM carbide in the inner core as was performed by Nakajima *et al.* [2011]

**Figure 9.** Axial compressibility of PM Fe₃C along 298 K isotherm. VR fits for all axes are shown.

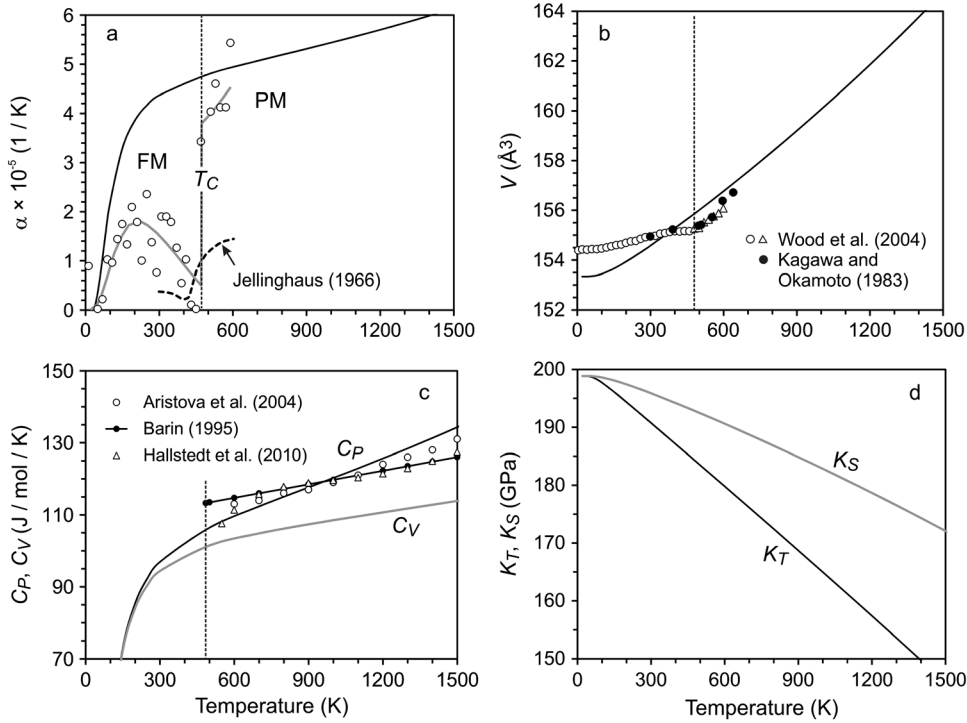


Figure 10. Calculated thermoelastic parameters of PM Fe_3C at 1 bar pressure (solid curves, this study) in comparison with reference data. (a) Thermal expansion coefficient (bold line), circles and grey line show data from [Wood et al., 2004; Aristova et al., 2004]; (b) Temperature dependence of unit cell volume; (c) heat capacities; and (d) bulk moduli.

for Fe_7C_3 because of the magnetic transition and clear differences in their compressibility. Taking into account minor differences in volume change across the PM-NM transition, we can assume that thermal properties of PM- Fe_3C can be very similar to those of NM- Fe_3C . At present, this is the only possible way to extrapolate the thermoelastic data for Fe_3C to inner core pressure. Similar assumptions for NM- Fe_7C_3 were considered by Chen et al. [2012].

[20] Figure 13 shows the comparison of Fe-carbides and hcp-Fe with the density of the core according to the PREM

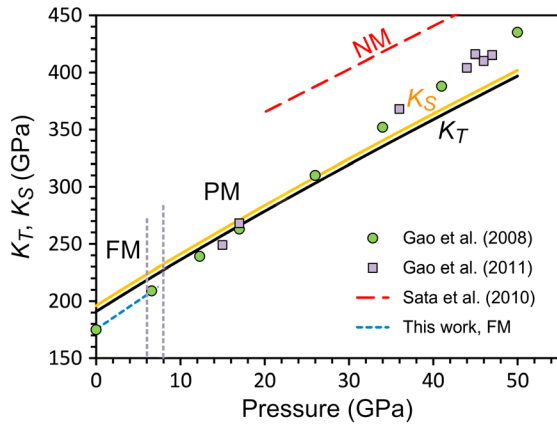


Figure 11. Pressure dependence of bulk moduli of Fe_3C from this study (black and orange solid lines) in comparison with reference data based on X-ray diffraction [Sata et al., 2010] and nuclear resonant inelastic X-ray scattering measurements [Gao et al., 2008; 2011].

model [Dziewonski and Anderson, 1981]. Calculated densities at 1 atm are 7.717 g/cm^3 for the PM-phase and 7.979 g/cm^3 for the NM-phase of Fe_3C . According to Sata et al. [2010], NM-phase has lower compressibility than the PM-phase (Table 2). However, calculated densities at 2898 K at inner core conditions (Figure 13) are almost similar with extrapolation error of about 0.2 g/cm^3 . Accordingly, high-temperature isotherms would also be nearly similar. This is not the case for Fe_7C_3 . The extrapolation of elasticity data for PM- and NM-phase of Fe_7C_3 to inner core conditions shows the difference in density of 1.5 cm^3 [Chen et al., 2012]. Accordingly, their high-temperature isotherms will also be significantly different.

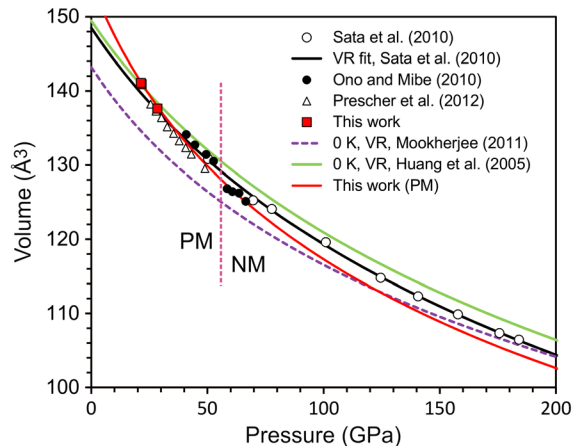


Figure 12. Compressibility of Fe_3C up to 200 GPa.

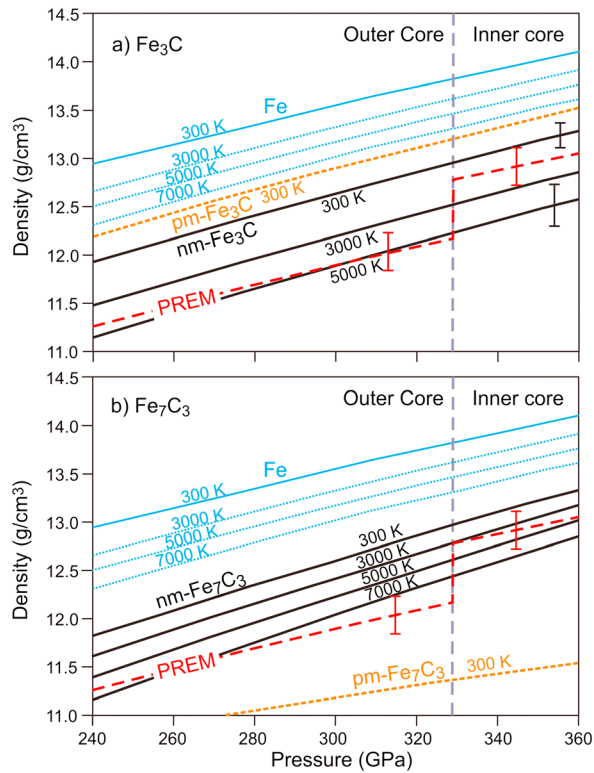


Figure 13. Calculated density of (a) Fe_3C and (b) Fe_7C_3 at the Earth's core conditions. For NM- Fe_3C , we used compressibility data from Sata *et al.* [2010] and thermal parameters of PM phase from this work. For NM- Fe_7C_3 , we used compressibility data from Chen *et al.* [2012] and thermal parameters for PM phase [Nakajima *et al.*, 2011]. Profiles for hcp-Fe are shown using parameters listed in Seagle *et al.* [2006]. The PREM profile is after Dziewonski and Anderson [1981]. The error bars for Fe_3C and PREM are shown.

At the outer-inner core boundary, the density at 298 K will be (g/cm^3) 13.8 for hcp-Fe, 12.95 for NM- Fe_7C_3 (6.2% density reduction), and 12.8 for NM- Fe_3C (7.2% density reduction). We should also note that high-temperature isotherms at 3000 and 5000 K in the inner core for Fe_3C and Fe_7C_3 are significantly different (Figure 13) due to different $\partial K_T/\partial T$ between the phases (-0.045 for PM-phase Fe_7C_3 [Nakajima *et al.*, 2011]).

[21] An assumption that the inner core consists of mixture of Fe (without Ni) and Fe-carbide provides an outer-inner core boundary temperature of 5000–7000 K [Nakajima *et al.*, 2011; Chen *et al.*, 2012]. The estimation of the carbon content in the inner core based on thermoelastic data for Fe_7C_3 corresponds to 6.5 ± 2.0 and 4.9 ± 1.8 wt % at 5000 and 7000 K, respectively [Nakajima *et al.*, 2011; Chen *et al.*, 2012]. Similar calculations for NM- Fe_3C indicate 3.3 ± 0.9 and 2.3 ± 0.8 wt % C for 5000 and 7000 K, respectively. Taking into account recent data on the stability of NM- Fe_3C at the core conditions [Takahashi *et al.*, 2012] these estimations would correspond to the maximum carbon content in the Earth's inner core. In order to place tighter constraints on the carbon content of the inner and outer cores, thermal EOS data of NM- Fe_3C under relevant pressures are required. In a recent comprehensive review that integrates constraints from mineral physics,

geochemistry, and cosmochemistry [Wood *et al.*, 2013] the carbon content of the core was estimated at the 1 wt% level.

6. Conclusions

[22] In this work we represent the first P - V - T equation of state for Fe_3C obtained using the multi-anvil technique and synchrotron radiation at pressures up to 31 GPa and temperatures up to 1473 K. As a note of caution, magnetic transitions at 8–10 and 55–60 GPa would introduce uncertainties into the calculation of thermodynamic parameters of Fe carbides and especially for extrapolation of the data to core-mantle boundary and inner core conditions. A fit of the P - V - T data was completed using Mie-Grüneisen-Debye EOS and the newly suggested Kunc-Einstein EOS, which allows for the calculation of all thermodynamic parameters necessary to calculate free energy at high P - T -conditions. We propose to use our present data for any thermodynamic calculations of chemical equilibria involving Fe_3C at pressures of PM-NM transition at 25–30 GPa.

[23] Assuming carbon as a sole light element in the system extrapolation of our data for equation of state to the NM-phase of Fe_3C indicate 3.3 ± 0.9 wt % C at 5000 K and 2.3 ± 0.8 wt % C at 7000 K at depths close to the inner core boundary. However, for accurate determination of the possible carbon concentrations in the core by comparison with inner core properties, we need to obtain experimental (in diamond anvil cell) of theoretical high-pressure and high-temperature EOSes for the NM phases of Fe carbides.

[24] **Acknowledgments.** We thank the reviewers for critical comments and suggestions and Matthew Karl for editing the manuscript for English and clarity. This work was supported by the Ministry of Education and Science of Russian Federation, projects 14.B37.21.0457 and 14.B25.31.0032 and conducted as a part of the Global Center-of-Excellence Program “Global Education and Research Center for Earth and Planetary Dynamics” at Tohoku University. It is partially supported by Integration project of Siberian Branch RAS 97 for 2012–2014 and Russian Foundation for Basic Research (12-05-33008). J.L. acknowledges support from CDAC, NSF EAR-1025629, and EAR-1291881 grants. Experiments were conducted under “SPRING-8” general research proposals 2009A1278, 2009B1327, and 2012B1289.

References

- Acet, M., B. Gehrmann, E. F. Wassermann, H. Bach, and W. Pepperhoff (2001), Relevance of magnetic instabilities to the properties of interstitial solid solutions and compounds of Fe, *J. Magn. Magn. Mater.*, 232(3), 221–230.
- Anderson, O. L. (1995), *Equations of State of Solids for Geophysics and Ceramic Science*, pp. 405, Oxford Univ. Press, Oxford.
- Anderson, O. L., and D. G. Isaak (2002), Another look at the core density deficit of Earth's outer core, *Phys. Earth Planet. Inter.*, 131(1), 19–27.
- Aristova, N. M., A. V. Gusarov, and V. Y. Leonidov (2004), Thermodynamic properties of individual substances, http://www.chem.msu.su/Zn/Fe/Fe3C_c.html, Electronic resource, Moscow Univ, Moscow.
- Barin, I. (1995), *Thermochemical Data of Pure Substances*, 1885 pp., VCH Verlagsgesellschaft mbH, Weinheim, Germany.
- Bazhanova, Z. G., A. R. Oganov, and O. Gianola (2012), Fe-C and Fe-H systems at pressures of the Earth's inner core, *Phys.-Uspekhi*, 55(5), 489–497.
- Belikov, A. M., and A. A. Savinskaya (1962), Anisotropy of thermal vibrations of atoms in cementite crystals, *Phys. Met. Met. Working (Fizika Metallov i Metallovedenie)*, 14, 299–301.
- Birch, F. (1964), Density and composition of mantle and core, *J. Geophys. Res.*, 69(20), 4377–4388.
- Chabot, N. L., A. J. Campbell, W. F. McDonough, D. S. Draper, C. B. Agee, M. Humayun, H. C. Watson, E. Cottrell, and S. A. Saslow (2008), The Fe-C system at 5 GPa and implications for Earth's core, *Geochim. Cosmochim. Acta*, 72(16), 4146–4158.
- Chen, B., L. Gao, B. Lavina, P. Dera, E. E. Alp, J. Zhao, and J. Li (2012), Magneto-elastic coupling in compressed Fe_7C_3 supports carbon in Earth's inner core, *Geophys. Res. Lett.*, 39, L18301, doi:10.1029/2012gl052875.
- Chipman, J. (1972), Thermodynamics and phase diagram of the Fe-C system, *Metall. Mater. Trans.*, 3, 55–64.

- Dodd, S. P., G. A. Saunders, M. Cankurtaran, B. James, and M. Acet (2003), Ultrasonic study of the temperature and hydrostatic-pressure dependences of the elastic properties of polycrystalline cementite (Fe₃C), *Phys. Status Solidi A*, 198(2), 272–281.
- Dorogokupets, P. I., and A. Dewaele (2007), Equations of state of MgO, Au, Pt, NaCl-B1, and NaCl-B2: Internally consistent high-temperature pressure scales, *High Pressure Res.*, 27(4), 431–446.
- Dorogokupets, P. I., and A. R. Oganov (2007), Ruby, metals, and MgO as alternative pressure scales: A semiempirical description of shock-wave, ultrasonic, x-ray, and thermochemical data at high temperatures and pressures, *Phys. Rev. B*, 75(2), 024115, doi:10.1103/PhysRevB.75.024115.
- Dubrovinsky, L. S., S. K. Saxena, N. A. Dubrovinskaya, S. Rekh, and T. le Bihan (2000), Gruneisen parameter of epsilon-iron up to 300 GPa from in-situ X-ray study, *Am. Mineral.*, 85(2), 386–389.
- Duman, E., M. Acet, E. F. Wassermann, J. P. Itie, F. Baudalet, O. Mathon, and S. Pascarelli (2005), Magnetic instabilities in Fe₃C cementite particles observed with FeK-edge X-ray circular dichroism under pressure, *Phys. Rev. Lett.*, 94(7), 075502, doi:10.1103/PhysRevLett.94.075502.
- Dziewonski, A. M., and D. L. Anderson (1981), Preliminary reference Earth model, *Phys. Earth Planet. Inter.*, 25, 297–356.
- Fiquet, G., J. Badro, F. Guyot, H. Requardt, and M. Krisch (2001), Sound velocities in iron to 110 gigapascals, *Science*, 291(5503), 468–471.
- Fiquet, G., J. Badro, E. Gregoryanz, Y. Fei, and F. Occelli (2009), Sound velocity in iron carbide (Fe₃C) at high pressure: Implications for the carbon content of the Earth's inner core, *Phys. Earth Planet. Inter.*, 172(1–2), 125–129.
- Gao, L., et al. (2008), Pressure-induced magnetic transition and sound velocities of Fe₃C: Implications for carbon in the Earth's inner core, *Geophys. Res. Lett.*, 35, L17306, doi:10.1029/2008gl034817.
- Gao, L., B. Chen, J. Zhao, E. E. Alp, W. Sturhahn, and J. Li (2011), Effect of temperature on sound velocities of compressed Fe₃C, a candidate component of the Earth's inner core, *Earth Planet. Sci. Lett.*, 309(3–4), 213–220.
- Gustafson, P. (1985), A thermodynamic evaluation of the Fe-C system, *Scand. J. Metall.*, 14, 259–267.
- Hallstedt, B., D. Djurovic, J. von Appen, R. Dronskowski, A. Dick, F. Koermann, T. Hickel, and J. Neugebauer (2010), Thermodynamic properties of cementite (Fe₃C), *Calphad*, 34(1), 129–133.
- Huang, L., N. V. Skorodumova, A. B. Belonoshko, B. Johansson, and R. Ahuja (2005), Carbon in iron phases under high pressure, *Geophys. Res. Lett.*, 32, L21314, doi:10.1029/2005gl024187.
- Jackson, I., and S. M. Rigden (1996), Analysis of P-V-T data: Constraints on the thermoelastic properties of high-pressure minerals, *Phys. Earth Planet. Inter.*, 96, 85–112.
- Jellinghaus, W. (1966), Massive cementite, *Arch. Eisenhuet.*, 37, 181.
- Kagawa, A., and T. Okamoto (1983), Hot hardness of cementite, *J. Mater. Sci.*, 18(1), 225–230.
- Katsura, T., K. Funakoshi, A. Kubo, N. Nishiyama, Y. Tange, Y. Sueda, T. Kubo, and W. Utsumi (2004), A large-volume high-pressure and high-temperature apparatus for in situ X-ray observation, 'SPEED-Mk.II', *Phys. Earth Planet. Inter.*, 143–144(1–4), 497–506.
- Komabayashi, T., and Y. W. Fei (2010), Internally consistent thermodynamic database for iron to the Earth's core conditions, *J. Geophys. Res.*, 115, B03202, doi:10.1029/2009jb006442.
- Kunc, K., I. Loa, and K. Syassen (2003), Equation of state and phonon frequency calculations of diamond at high pressures, *Phys. Rev. B*, 68(9), 094107, doi:10.1103/PhysRevB.68.094107.
- Li, J., and Y. Fei (2003), Experimental constraints on core composition, in *Treatise on Geochemistry*, edited by H. D. Holland and K. K. Turekian, pp. 521–546, Elsevier - Pergamon, Oxford.
- Li, J., H. K. Mao, Y. Fei, E. Gregoryanz, M. Eremets, and C. S. Zha (2002), Compression of Fe₃C to 30 GPa at room temperature, *Phys. Chem. Miner.*, 29(3), 166–169.
- Lin, J. F., V. V. Struzhkin, H. K. Mao, R. J. Hemley, P. Chow, M. Y. Hu, and J. Li (2004), Magnetic transition in compressed Fe₃C from X-ray emission spectroscopy, *Phys. Rev. B*, 70(21), 212405, doi:10.1103/PhysRevB.70.212405.
- Lin, J. F., W. Sturhahn, J. Y. Zhao, G. Y. Shen, H. K. Mao, and R. J. Hemley (2005), Sound velocities of hot dense iron: Birch's law revisited, *Science*, 308(5730), 1892–1894.
- Litasov, K., E. Ohtani, A. Sano, A. Suzuki, and K. Funakoshi (2005), In situ X-ray diffraction study of post-spinel transformation in a peridotite mantle: Implication for the 660-km discontinuity, *Earth Planet. Sci. Lett.*, 238(3–4), 311–328.
- Litasov, K. D., E. Ohtani, S. Ghosh, Y. Nishihara, A. Suzuki, and K. Funakoshi (2007), Thermal equation of state of superhydrox phase B to 27 GPa and 1373 K, *Phys. Earth Planet. Inter.*, 164(3–4), 142–160.
- Litasov, K. D., E. Ohtani, Y. Nishihara, A. Suzuki, and K. Funakoshi (2008), Thermal equation of state of Al- and Fe-bearing phase D, *J. Geophys. Res.*, 113, B08205, doi:10.1029/2007jb004937.
- Litasov, K. D., et al. (2013), Thermal equation of state and thermodynamic properties of Molybdenum at high pressure, *J. Appl. Phys.*, 113, 093507, doi:10.1063/1.4794127.
- Lord, O. T., M. J. Walter, R. Dasgupta, D. Walker, and S. M. Clark (2009), Melting in the Fe-C system to 70 GPa, *Earth Planet. Sci. Lett.*, 284(1–2), 157–167.
- Mookherjee, M. (2011), Elasticity and anisotropy of Fe₃C at high pressures, *Am. Mineral.*, 96(10), 1530–1536.
- Mookherjee, M., Y. Nakajima, G. Steinle-Neumann, K. Glazyrin, X. Wu, L. Dubrovinsky, C. McCammon, and A. Chumakov (2011), High-pressure behavior of iron carbide (Fe₇C₃) at inner core conditions, *J. Geophys. Res.*, 116, B04201, doi:10.1029/2010jb007819.
- Nakajima, Y., E. Takahashi, T. Suzuki, and K. Funakoshi (2009), "Carbon in the core" revisited, *Phys. Earth Planet. Inter.*, 174(1–4), 202–211.
- Nakajima, Y., E. Takahashi, N. Sata, Y. Nishihara, K. Hirose, K. Funakoshi, and Y. Ohishi (2011), Thermoelastic property and high-pressure stability of Fe₇C₃: Implication for iron-carbide in the Earth's core, *Am. Mineral.*, 96(7), 1158–1165.
- Ono, S., and K. Mibe (2010), Magnetic transition of iron carbide at high pressures, *Phys. Earth Planet. Inter.*, 180(1–2), 1–6.
- Poirier, J. P. (1994), Light elements in the Earth's outer core: A critical review, *Phys. Earth Planet. Inter.*, 85(3–4), 319–337.
- Poirier, J. P. (2000), *Introduction to the Physics of the Earth's Interior*, 2nd ed., 312 pp., Cambridge Univ. Press, Cambridge, U. K.
- Prescher, C., L. Dubrovinsky, C. McCammon, K. Glazyrin, Y. Nakajima, A. Kantor, M. Merlini, and M. Hanfland (2012), Structurally hidden magnetic transitions in Fe₃C at high pressures, *Phys. Rev. B*, 85(14), 140402, doi:10.1103/PhysRevB.85.140402.
- Sata, N., K. Hirose, G. Shen, Y. Nakajima, Y. Ohishi, and N. Hirao (2010), Compression of FeSi, Fe₃C, Fe_{0.95}O, and FeS under the core pressures and implication for light element in the Earth's core, *J. Geophys. Res.*, 115, B09204, doi:10.1029/2009jb006975.
- Scott, H. P., Q. Williams, and E. Knittle (2001), Stability and equation of state of Fe₃C to 73 GPa: Implications for carbon in the Earth's core, *Geophys. Res. Lett.*, 28(9), 1875–1878.
- Seagle, C. T., A. J. Campbell, D. L. Heinz, G. Shen, and V. B. Prakapenka (2006), Thermal equation of state of Fe₃S and implications for sulfur in Earth's core, *J. Geophys. Res.*, 111, B06209, doi:10.1029/2005jb004091.
- Shatskiy, A., I. S. Sharygin, P. N. Gavryushkin, K. D. Litasov, Y. M. Borzdov, A. V. Shcherbakova, Y. Higo, K. Funakoshi, Y. N. Palyanov, and E. Ohtani (2013), The system K₂CO₃-MgCO₃ at 6 GPa and 900–1450°C, *Am. Mineral.*, 98, 1593–1603.
- Sokolova, T. S., P. I. Dorogokupets, and K. D. Litasov (2013), Self-consistent pressure scales based on the equations of state for ruby, diamond, MgO, B₂-NaCl, as well as Au, Pt and other metals to 4 Mbars and 3000 K, *Russ. Geol. Geophys.*, 54(2), 181–199.
- Stevenson, D. J. (1981), Models of the Earth's core, *Science*, 214(4521), 611–619.
- Stixrude, L., E. Wasserman, and R. E. Cohen (1997), Composition and temperature of Earth's inner core, *J. Geophys. Res.*, 102(B11), 24,729–24,739.
- Strong, H. M., and R. M. Chrenko (1971), Further studies on diamond growth rates and physical properties of laboratory-made diamonds, *J. Phys. Chem.*, 75, 1838–1843.
- Takahashi, S., E. Ohtani, T. Sakai, N. Hirao, and Y. Ohishi (2012), Stability and melting of Fe₃C at high pressure and temperature: Implication for the carbon in the Earth's core, Abst. of 2012 Fall Meeting, American Geophysical Union, San Francisco, USA, MR11B-2489.
- Tsuzuki, A., S. Sago, and S. I. Hirano (1984), High-temperature and pressure preparation and properties of iron carbides Fe₇C₃ and Fe₃C, *J. Mater. Sci.*, 19(8), 2513–2518.
- Utsumi, W., K. Funakoshi, S. Urakawa, M. Yamakata, K. Tsuji, H. Konishi, and O. Shimomura (1998), SPring-8 beamlines for high pressure science with multi-anvil apparatus, *Rev. High Pressure Sci. Technol.*, 7, 1484–1486.
- Vinet, P., J. Ferrante, J. H. Rose, and J. R. Smith (1987), Compressibility of solids, *J. Geophys. Res.*, 92, 9319–9325.
- Vocadlo, L., J. Brodholt, D. P. Dobson, K. S. Knight, W. G. Marshall, G. D. Price, and I. G. Wood (2002), The effect of ferromagnetism on the equation of state of Fe₃C studied by first-principles calculations, *Earth Planet. Sci. Lett.*, 203(1), 567–575.
- Weerasinghe, G. L., R. J. Needs, and C. J. Pickard (2011), Computational searches for iron carbide in the Earth's inner core, *Phys. Rev. B*, 84(17), 174110, doi:10.1103/PhysRevB.84.174110.
- Wood, B. J. (1993), Carbon in the core, *Earth Planet. Sci. Lett.*, 117(3–4), 593–607.
- Wood, I. G., L. Vocadlo, K. S. Knight, D. P. Dobson, W. G. Marshall, G. D. Price, and J. Brodholt (2004), Thermal expansion and crystal structure of cementite, Fe₃C, between 4 and 600 K determined by time-of-flight neutron powder diffraction, *J. Appl. Crystallogr.*, 37, 82–90.
- Wood, B. J., J. Li, and A. Shahar (2013), Carbon in the Core: Its influence on the properties of core and mantle, *Rev. Mineral. Geochem.*, 75(1), 231–250.
- Yamazaki, D., E. Ito, T. Yoshino, A. Yoneda, X. Guo, B. Zhang, W. Sun, A. Shimojuku, N. Tsujino, and T. Kunimoto (2012), P-V-T equation of state for epsilon-iron up to 80 GPa and 1900 K using the Kawai-type high pressure apparatus equipped with sintered diamond anvils, *Geophys. Res. Lett.*, 39, L20308, doi:10.1029/2012gl053540.